

An Injectable Composite Bone Cement Based on Mesoporous Borosilicate Bioactive Glass Spheres

CHANG Yuchen¹, LIN Ziyang¹, XIE Xin¹, WU Zhangfan¹, YAO Aihua¹,
YE Song¹, LIN Jian¹, WANG Deping¹, CUI Xu²

(1. School of Materials Science and Engineering, Tongji University, Shanghai 201804, China; 2. Center for Human Tissues and Organs Degeneration, Institute of Biomedicine and Biotechnology, Shenzhen Institutes of Advanced Technology, Chinese Academy of Science, Shenzhen 518055, China)

Abstract: An injectable composite bone cement was fabricated by employing Sol-Gel derived mesoporous borosilicate bioactive glass spheres (MBGS) as solid phase and sodium alginate (SA) solution as liquid phase. The effects of the B₂O₃/SiO₂ ratio in MBGS on its textural properties and workability, compressive strength and bioactivity of bone cement were characterized. It is found that with the increase of boron content, the specific surface area of MBGS increases from 161.71 m²/g to 214.28 m²/g, and the average pore size and total pore volume also increase, which accelerates the Ca²⁺ release and rapidly crosslinks MBGS and SA. Thus, the workability, mechanical property and *in vitro* mineralization of bone cement are significantly improved, as the setting time is shortened from 21 min to 9 min and the compressive strength is enhanced from 3.4 MPa to 4.1 MPa. Comprehensive performance of all aspects, BC-30 bone cement showing good workability, mechanical properties and *in vitro* mineralization ability, displays the optimal component. Therefore, improving the textural properties of MBGS is an effective method to enhance the workability, compressive strength and bioactivity of composite bone cement.

Key words: injectable bone cement; mesoporous borosilicate bioactive glass; bioactivity; workability

In the treatment of bone defect and fracture, injectable bone cements have been widely used due to their excellent plasticity and formability, which make them easy to match irregular bone defects and avoid gaps between the implant and the bone^[1]. Additionally, bone cement can be implanted by minimally invasive procedures and self-cured *in situ*, which means less pain, quicker recovery and low risk of infection^[2]. Commercially available bone cements such as poly(methyl methacrylate) (PMMA) cement, calcium sulfate cement (CSC) and calcium phosphate cement (CPC) have been clinically used^[3-7]. As an emerging type of bone repair material, bioactive glass bone cement exhibits superior to other candidate materials in regard to bioactivity, osteoconductivity and osteoinductivity^[8]. Recent study confirmed that the initial particle size of bioactive glass powders had a significant effect on the resultant cement properties, and nanopowder-derived cements exhibited high surface area, and therefore

desired workability and accelerated angiogenesis and osteogenesis were achieved^[9-10].

Injectable cements composed of borate bioactive glass are a new class of bone substitutes which have good mechanical and handling properties^[11], and also receive an increasing research interest over the last decade, owing to the high reactivity and stimulation effect on angiogenesis and osteogenesis of borate bioactive glass^[12-13]. Moreover, introducing a porous structure to borate glass can accelerate the degradation and mineralization of bone cement^[14]. Additionally, since the boron level in blood is about 0.14 and 0.90 µg/L in bone^[15], a proper amount of boron released into the tissue microenvironment during degradation has an important role in mineralization and prevention of osteoporosis^[16-17]. Due to the boron-oxygen trihedral structure^[18-19], borate glass has lower stability than silicate glass which causes a higher degradation rate. However, excessive degradation of boron glass can also

Received date: 2020-03-17; **Revised date:** 2020-04-09

Foundation item: National Key Research and Development Program of China (2018YFC1106302); National Natural Science Foundation of China (51772210, 51802340, 31870956, 81672227); Science and Technology Project of Guangdong Province-Doctoral Startup Fund of 2017 (2017A030310318)

Biography: CHANG Yuchen(1995-), female, Master candidate. E-mail: changyuchencccc@163.com
常宇辰(1995-), 女, 硕士研究生. E-mail: changyuchencccc@163.com

Corresponding author: WANG Deping, professor. E-mail: wdpskh@tongji.edu.cn; CUI Xu, PhD. E-mail: xu.cui@siat.ac.cn
王德平, 教授. E-mail: wdpskh@tongji.edu.cn; 崔旭, 博士. E-mail: xu.cui@siat.ac.cn

cause problems of cytotoxicity^[20]. By comparison, borosilicate glasses can not only allow to control the degradation rate over a wide range, but also avoid the cytotoxicity problem. What's more, under dynamic conditions, an increase in boron content will not cause the bioactive glass to exhibit significant cytotoxicity^[21]. It was reported that after 2.1 mg of boron intravenously injected into mice, the blood boron level was initially 158 and 40 $\mu\text{g/L}$ after 2 h which meant boron was rapidly eliminated under the dynamic condition^[15]. Therefore, the development of an injectable composite bone cement composed of mesoporous borosilicate bioactive glass spheres deserves exploring.

With a higher specific surface area and reactivity, mesoporous borosilicate bioactive glass nanoparticles process a higher Ca^{2+} release, which may accelerate the ionic cross-linking reaction between borosilicate glass and sodium alginate solution^[22]. Therefore, the objective of this study was to investigate the development of an injectable composite bone cement composed of mesoporous borosilicate bioactive glass spheres (MBGS) dispersed in modified sodium alginate solution that served as the setting liquid, and improve the workability and bioactivity of bone cement. The MBGS was fabricated *via* Sol-Gel method using cetyltrimethyl ammonium bromide (CTAB) as a template. A sodium alginate solution was selected based on its setting characteristics and its biocompatibility *in vivo*^[23]. The effect of $\text{B}_2\text{O}_3/\text{SiO}_2$ ratio of the MBGS on their textural properties, and consequently on the workability, compressive strength and bioactivity of the resultant bone cements were evaluated.

1 Materials and methods

1.1 Materials

Tributyl borate (TBB), tetraethyl orthosilicate (TEOS), cetyltrimethyl ammonium bromide (CTAB), triethylphosphate (TEP), calcium nitrate tetrahydrate (CN), absolute ethanol, deionized water, ammonia solution (25wt% NH_3 in water), sodium hydrogen phosphate (Na_2HPO_4), *D*-gluconic acid *d*-lactone (GDL) and sodium alginate (SA) were purchased from Sinopharm Chemical Reagent Co., Ltd (Shanghai, China). All chemical reagents were chemical grade.

1.2 Preparation and characterization of mesoporous borosilicate bioactive glass spheres (MBGS)

The mesoporous borosilicate bioactive glass spheres were synthesized by Sol-Gel method using CTAB as template. 0.14 g CTAB was dissolved in a mixture containing 40 mL absolute ethanol and 60 mL deionized water under stirring at 40 $^{\circ}\text{C}$ until CTAB completely dissolved. Then a certain amount of TBB and TEOS

were then added into the solution. Subsequently 0.50 mL ammonia, 0.30 mL TEP and 1.913 g CN were separately added into the solution at 30 min intervals. After stirred for another 1.5 h, the resulting solution was centrifuged to collect the white precipitate. Thereafter, the white precipitate was further washed three times with absolute ethanol and deionized water and dried at 60 $^{\circ}\text{C}$ for 24 h. The MBGS powders were eventually obtained after removal of remaining organics by sintering at 450 $^{\circ}\text{C}$ for 3 h (1 $^{\circ}\text{C}/\text{min}$). Three MBGS samples with various $\text{B}_2\text{O}_3/\text{SiO}_2$ ratios were designated as MBGS-20, MBGS-30, and MBGS-40, and their corresponding compositions were shown in Table 1.

The phase composition and microstructure of the MBGS were analyzed using X-ray diffractometer (XRD, D/max2550, Rigaku Co., Japan), and transmission electron microscope (TEM, JEM2100, JEOL Co., Japan). N_2 adsorption-desorption isotherms were performed at 77 K using a NOVA 2200e (Quantachrome Instruments Co., America). The specific surface area and pore volume were calculated from N_2 adsorption data in the partial relative pressure range of 0.05–0.35 using the Brunauer-Emmette-Teller (BET) method^[24] and the pore size distribution was analyzed from adsorption data in the partial relative pressure range of 0.35–0.98 using the Barrette-Joynere-Halenda (BJH) method^[25].

1.3 Fabrication of MBGS/SA composite bone cements

The SA liquid phase was firstly prepared by dissolving 2 g SA, 1 g *D*-gluconic acid *d*-lactone and 3 g sodium hydrogen phosphate in 100 mL deionized water. The MBGS-20, MBGS-30, and MBGS-40 powders were separately mixed with the liquid phase at a liquid/solid ratio of 0.75 mL/g to fabricate MBGS/SA composite bone cements. The resultant three bone cement samples were designated as BC-20, BC-30, and BC-40, respectively.

1.4 Evaluation of the workability of the MBGS/SA composite bone cements

The injectability of the MBGS/SA composite bone cements were evaluated *in vitro* using a procedure described previously^[26]. Bone cement pastes were placed into the syringe fitted with a needle of 1.7 mm inner diameter. Then the pastes were extruded out of the syringe at a crosshead speed of 15 mm/min until the maximum force reached 100 N. During the extrusion procedure

Table 1 The compositions of MBGS/mol%

| Glass | B_2O_3 | SiO_2 | CaO | P_2O_5 |
|---------|------------------------|----------------|-----|------------------------|
| MBGS-20 | 20 | 40 | 36 | 4 |
| MBGS-30 | 30 | 30 | 36 | 4 |
| MBGS-40 | 40 | 20 | 36 | 4 |

the extrusion force-displacement curve was recorded for each group of composite bone cement pastes. The injectability was calculated according to the following equation^[27]:

$$\text{Injectability} = M_1 / M_0 \times 100\% \quad (1)$$

where M_0 is the original mass of the paste; M_1 is the mass of the paste extruded from the syringe.

The initial setting time of the bone cement paste determined according to ISO9917-1. A PMMA mold containing five cylindrical holes ($\phi 6$ mm \times 12 mm) was placed in a water bath at 37.8 °C. Then the cement paste (prepared as described earlier) was injected into the mold cavity. The setting time of the paste was determined using a Vicat's apparatus (1.13 mm diameter and 400 g weight)^[28]. The setting time of the paste was defined as the time from the beginning of the mixing of solid phase and liquid phase until the Vicat needle with a tip of 1 mm left no indentation on the surface of the paste. Three samples were tested and the setting time was determined as a mean \pm SD.

For compressive strength test, the bone cement pastes were cast into cylindrical Teflon mold and kept in an incubator at 37 °C and 100% relative humidity for 24 h to obtain cylindrical bone cement samples ($\phi 6$ mm \times 12 mm). Subsequently the compressive tests were performed using Electronic universal testing machine (CTM2500, Xie Qiang Instrument Manufacturing (Shanghai) Co. Ltd, China) at a constant cross head speed of 0.5 mm/min. Five samples of each cement were tested and the compressive strength was determined as a mean \pm SD.

The anti-washout property of the bone cements was measured by testing the remaining weight percentage after being shaken in phosphate buffer solution (PBS) for different times. The mass of the as-prepared cement paste was firstly weighted as M_0 . The sample was then carefully placed in a cup filled with PBS. The cup was put into a shaker and vibrated at a speed of 180 r/min and 37 °C for 2, 5, 12, 24 h. At each time, the amount of cement paste remaining was collected, freeze-dried and weighed as M_n ($n=2, 5, 12$ and 24). The remaining weight percentage was used to evaluate the anti-washout ability according to the following equation^[29]:

$$\text{Remaining weight percentage} = M_n / M_0 \times 100\% \quad (2)$$

1.5 Evaluation of biomineralization *in vitro*

The bioactivity of the MBGS/SA composite bone cements was studied by immersion in simulate body fluid (SBF) at 37 °C. Cylindrical samples of each cement ($\phi 6$ mm \times 12 mm) were set for 4 h and immersed in 10 mL SBF in polyethylene containers. After 14 d of immersion, the samples were removed, washed with deionized water, dried at 90 °C and weighed. The phase compositions of the

composite bone cements after being immersed in SBF were analyzed by X-ray diffraction (XRD) (D/max-2500VB2+/PC X-ray diffractometer) using graphite monochromatized CuK α radiation ($\lambda=0.15406$ nm) at a scanning rate of 10 (°)/min (in the range of 10°–80°). The morphological features of the composite bone cements before and after immersion in SBF were examined in a field emission scanning electron microscope (FESEM, Hitachi S-4700). The samples were sputter-coated with gold prior to examination.

2 Results and discussion

2.1 Textural properties of MBGS

The phase composition, morphology and microstructure of the as-prepared MBGS were determined using XRD, FT-IR, TEM and nitrogen adsorption and desorption isotherm analyses. The B₂O₃/SiO₂ ratio in the studied range had no effect on the phase composition (Fig. 1) and morphology (Fig. 2) of MBGS, and all three samples remained amorphous and display uniform and regular spherical morphologies. However, there was an increase in their specific surface area, average pore diameter and total pore volume with increasing boron content, as evidenced by the data in Table 2. Additionally, it was found from TEM images that mesoporous structure became more apparent for the samples with high boron content.

The microstructure of the MBGs with various B₂O₃/SiO₂ was determined by FT-IR spectra in Fig. 3. The main resonances consisted of the vibrational modes of the [SiO₄] and [BO₃] groups in the borosilicate glass network. The resonance at 1350–1450 cm⁻¹ and at 690–720 cm⁻¹

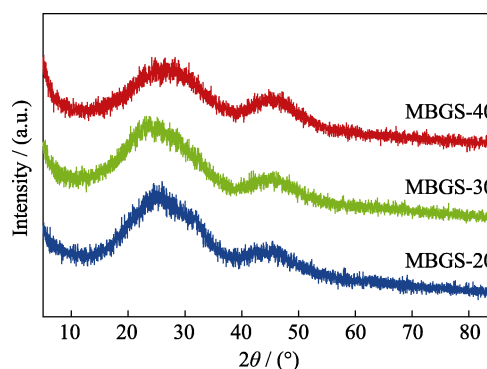


Fig. 1 XRD patterns of the as-prepared MBGS

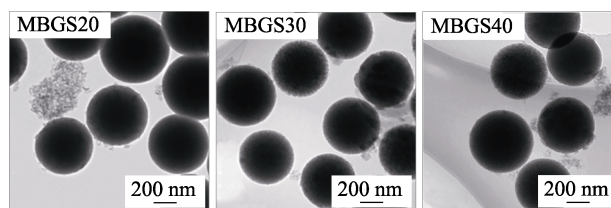


Fig. 2 TEM images of the as-prepared MBGS

Table 2 Specific surface area, average pore diameter and total pore volume of the three groups of MBGS

| Sample | Specific surface area/(m ² ·g ⁻¹) | Average pore diameter/nm | Total pore volume/(mL·g ⁻¹) |
|---------|--|--------------------------|---|
| MBGS-20 | 161.71 | 13.33 | 0.052 |
| MBGS-30 | 176.98 | 13.97 | 0.057 |
| MBGS-40 | 214.28 | 15.11 | 0.079 |

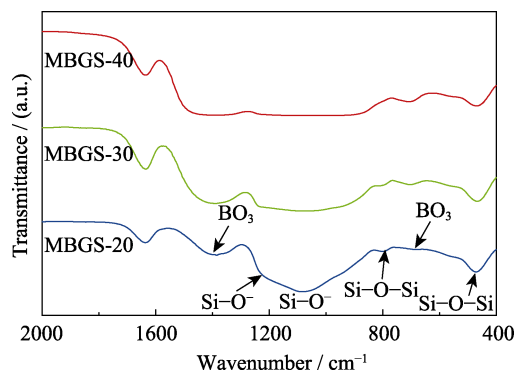
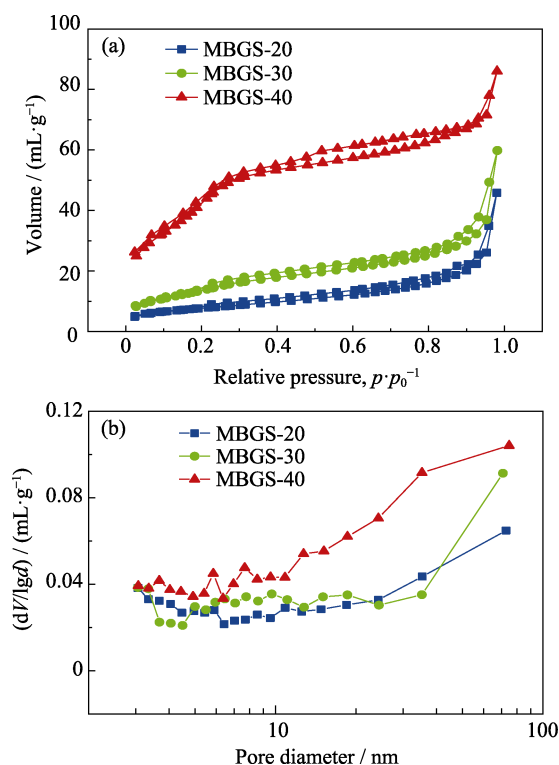


Fig. 3 FT-IR spectra of the as-prepared MBGS

were assigned to the B–O stretching and bending modes of BO_3 groups, respectively, while the resonances at 800 and 460 cm^{-1} were assigned to symmetric stretching mode and bending mode of $\text{Si-O-Si}^{[30]}$, respectively. In addition, the broad resonances centered at 1080 and 1220 cm^{-1} corresponding to the TO and LO modes of the asymmetric Si-O^- stretching vibration were also observed for the MBGS-20B sample^[31]. It is obvious that with the increasing boron content, the resonances of Si–O became weaker and the resonance corresponding BO_3 group became more pronounced, suggesting partial substitution of $[\text{SiO}_4]$ by $[\text{BO}_3]$. In the present work, the MBGs were produced by partially replacing the SiO_2 in Sol-Gel derived silicate 58S with B_2O_3 . In contrast to silicate-based Sol-Gels where the main network former tetrahedrally coordinated $[\text{SiO}_4]$ construct a strongly interconnected network, in borate-based glasses, the main structural units are BO_3 trihedron or chains of $[\text{BO}_3]$ triangles. The incorporation of threefold coordinated boron can therefore disrupt the silicate network, resulting in decreasing network connectivity^[32]. This indicates looser glass network, and thus higher surface area and larger pore volume.

The mesoporous structure of the MBGS was confirmed by nitrogen adsorption and desorption isotherms in Fig. 4. All three samples represented type IV isotherms which was typical for mesoporous materials^[33]. While all samples posed H2 type hysteresis loops, the MBGS-40 expressed a combination of H2 and H4 type loops, indicating that the sample contained both micropores and mesopores. The presence of micropores further suggested its highly porous network structure. The pore

Fig. 4 (a) N_2 adsorption-desorption isotherms and (b) pore size distributions of MBGS-20, MBGS-30, and MBGS-40

size distributions in Fig. 4 (b) showed that in addition to the mesopores that mainly distributed between 5 and 15 nm, there were still a large number of macropores (>50 nm) generated from the interspace between the particles. The presence of the high pressure region in Fig. 4 also supported this conclusion.

2.2 Microstructures of the MBGS/SA bone cements

To confirm the favorable roles of MBGS textural properties (specific surface area and pore volume), the surface and cross-sectional morphologies of the MBGS/SA bone cements were firstly observed. As shown in Fig. 5 (a-c), the three samples presented distinctly different surface morphologies. The bone cements with higher $\text{B}_2\text{O}_3/\text{SiO}_2$ ratio (BC-30 and BC-40) had a significantly larger number of interconnected pores, whereas BC-20 displayed relatively smooth surface. As indicated in our previous study^[26], Ca^{2+} ions released from the borosilicate glass participated in intermolecular cross-linking with the SA chains to form an insoluble Ca-SA hydrogel, leading to the hardening of the bone cements. In this study, a similar process occurred, yet at a more rapid rate compared to non-mesoporous particles-derived bone cement, which was attributable to their higher textural properties.

The increased $\text{B}_2\text{O}_3/\text{SiO}_2$ ratio caused poor chemical stability of the glass network and promoted the rapid degradation of MBGS. In our previous study, B ions

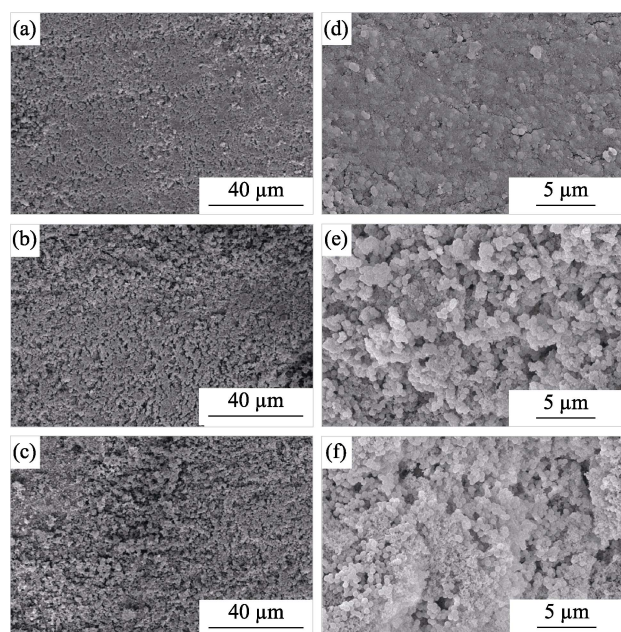


Fig. 5 SEM images of (a, d) BC-20, (b, e) BC-30, and (c, f) BC-40 bone cement specimens

accumulative concentration released from borosilicate bioactive bone cement with B_2O_3/SiO_2 ratio increasing during immersion was increased^[26], as well as the release of Ca^{2+} from the bioactive glass. With the increased specific surface area, MBGS can also allow for a more rapid release of ions. As a result, more SA molecules were consumed to react with the released Ca^{2+} , leading to the formation of highly cross-linked hydrogel network, as shown in Fig. 5 (e, f). Such a highly porous structure is beneficial to the cell penetration, vascularization, and nutrient supplying^[34]. Li, *et al.*^[35] has prepared mesoporous bioactive glass-PLGA composite scaffolds and illustrated that the scaffolds can achieve desirable vascularization and bone regeneration.

2.3 Setting properties

As shown in Fig. 6, since the B_2O_3/SiO_2 ratio was increased, the setting time was shortened from 21 min to 9 min, which was comparable to other cements and suitable for clinical applications. The compressive strength of the bone cements is slightly increased from (3.4 ± 0.2) MPa to (4.1 ± 0.3) MPa as the B_2O_3/SiO_2 ratio increased from 1 : 2 to 2 : 1, of which bone cement with B_2O_3/SiO_2 ratio at 2 : 1 is 2 times higher than that of the non-mesoporous-derived bone cements produced under the same conditions in our previous study^[26]. As the content of boron increased, the glass network became more unstable, resulting in the rapid release of Ca^{2+} ions and a more complete cross-link between glass and SA, which ultimately lead to higher compressive strength. However, the compressive strength still needs improvement which may be limited by the

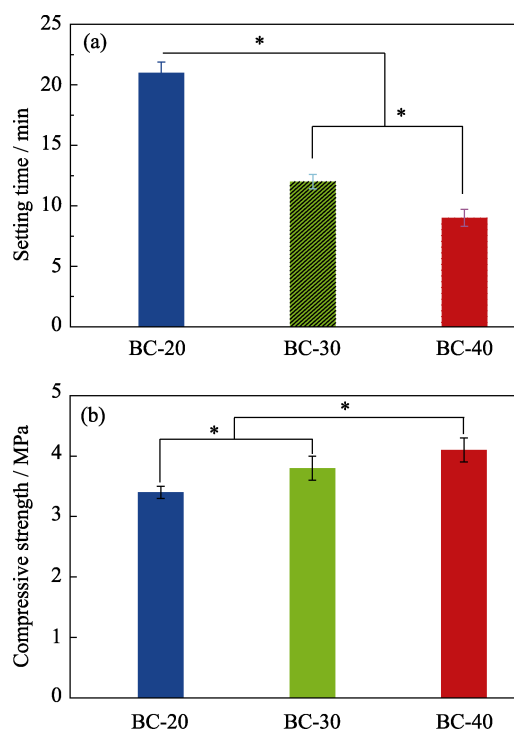


Fig. 6 (a) Setting time and (b) compressive strength of BC-20, BC-30, and BC-40, respectively

* indicates significant difference between groups, $p < 0.05$

degree of cross-linking between SA and glass. To further enhance the compressive strength of bone cement, adjusting the concentration of SA or adding bioactive fillers such as HA and bioglass fibers should be considered in the future study.

2.4 Injectability

Data from the injectability test showed that both BC-20 and BC-30 pastes could be extruded easily as confirmed by Fig. 7 and their injectability remained about 90% during the first 6 min, indicating their appropriate viscosity and excellent injectability. In comparison, larger force was required for the extrusion of the BC-40 paste, yet only 76wt% fraction was extruded. Additionally, since the viscosity of the BC-40 paste was too high to completely remove the incorporated bubbles, an abrupt drop in the extrusion force was observed on curve C in Fig. 7. The three pastes remained continuous and regular shape after extrusion as shown in Fig. 8. BC-20 and BC-30 pastes were quite soft and sticky, while the BC-40 paste was relatively dry, further indicating its high viscosity and poor injectability. The difference in the injectability of bone cements was due to the different texture structures of the Sol-Gel-derived borosilicate glasses. The higher specific surface area of MBGS-40 and subsequent rapid ions release resulted in a hydrogel network with higher cross-linked degree, which increases the viscosity of the paste, thereby encountering larger extrusion resistance.

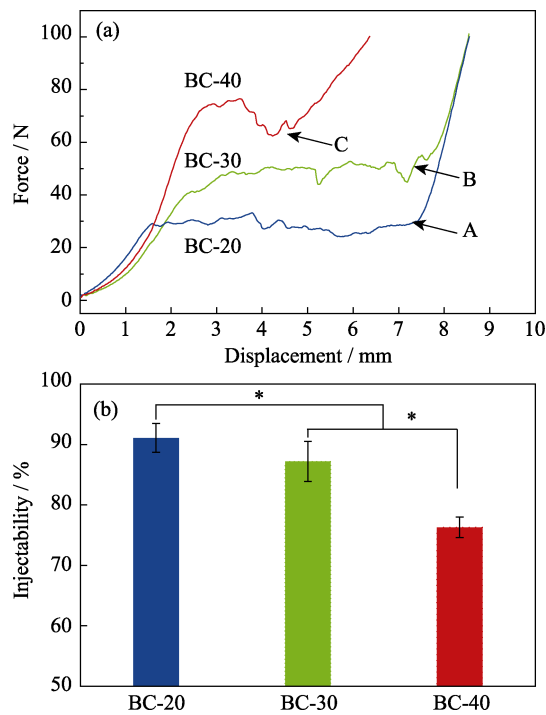


Fig. 7 (a) Force-displacement curves and (b) injectabilities of mesoporous borosilicate bone cements for different B_2O_3 contents

* indicates significant difference between groups, $p < 0.05$



Fig. 8 Photographs of the mesoporous borosilicate bone cement extruded from the syringe

2.5 Anti-washout property

The anti-washout property is an important parameter to evaluate the ability of bone cements to keep the initial shape in a dynamic aqueous environment^[36], which is vital to avoid the possible occurrence of inflammatory reactions resulted from the collapsing fragment of bone cements. The anti-washout property of all bone cements was assessed and the results were shown in Fig. 9. At the first 5 h, all specimens lost weight rapidly and then the weight loss gradually stabilized after 24 h. The remaining weight ratios were $(81.9 \pm 2.7)\%$, $(83.2 \pm 3.1)\%$, and $(87.1 \pm 2.4)\%$ for BC-20, BC-30, and BC-40, respectively, indicating that increasing B_2O_3 content in MBGS improved the anti-washout property of the bone cements. The gradual increase in resistance to collapse may be attributed to the faster cross-linking of bioactive glass and SA, as the boron content increased which leads to larger specific surface area of MBGS. Fig. 10 showed the shape changes of bone cement specimens after being shaken for different time periods. As observed, all

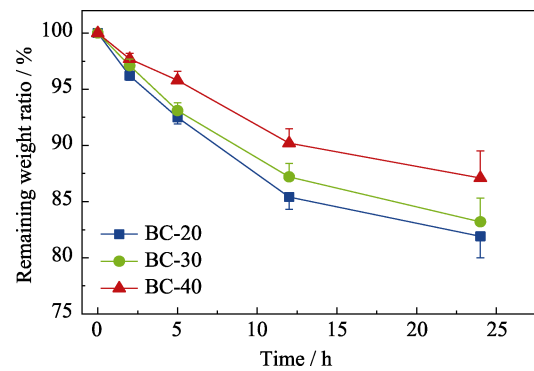


Fig. 9 Anti-washout properties of mesoporous borosilicate bone cements

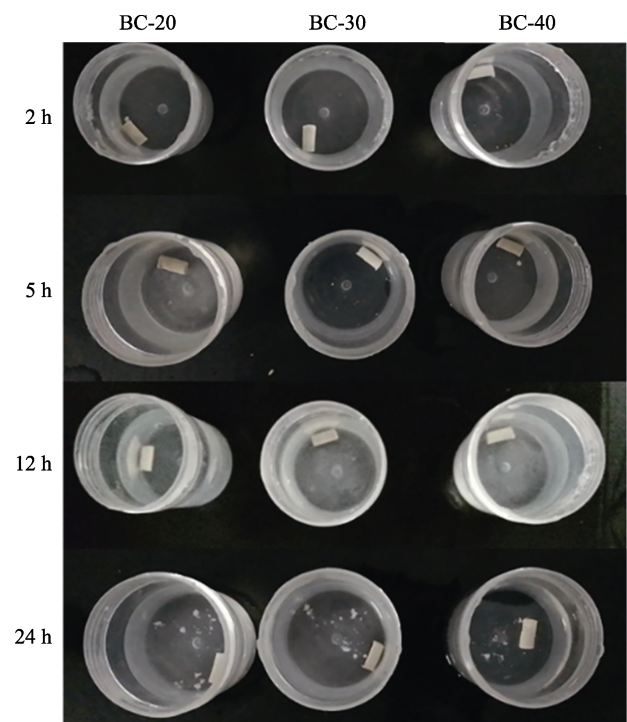


Fig. 10 Morphologies of mesoporous borosilicate bone cement specimens after being shaken in PBS at 37 °C for 2, 5, 12, and 24 h, respectively

specimens showed good resistance to disintegration, and they could maintain their original shape even under being shaken in PBS for 24 h.

2.6 Biomineralization ability *in vitro*

The mineralization ability of the bone cements was confirmed by using XRD, SEM and EDS analyses. In Fig. 11, after 3 d of immersion in SBF, weak diffraction peaks in XRD patterns corresponding to HA crystalline were presented, then the peaks became sharper and more defined over time, indicating the progressive crystallization of HA. The result demonstrated significantly more rapid HA formation compared with the bone cements produced from non-mesoporous borosilicate glass, attributable to the high surface area and porosity of the present MBGs coupled with rapid ion release. Wang,

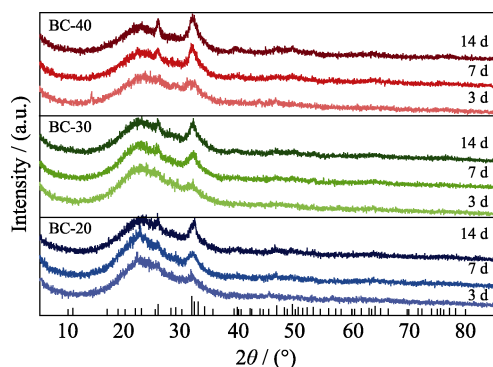


Fig. 11 XRD patterns of bone cement specimens after being immersed in SBF for 3, 7 and 14 d, respectively

et al.^[37] also successfully prepared radial mesoporous bioactive glass through wet chemical method and proved its excellent biomineralization properties. SEM images in Fig. 12 showed that the surfaces of all three samples were covered by a large amount of agglomerated HA particles after 14 d of immersion in SBF. Corresponding EDS spectra confirmed that the Ca/P ratios of the mineralization products were close to that of stoichiometric HA (Ca/P=1.67).

Consequently, BC-30 bone cement had appropriate setting time, injectability, anti-washout properties and mineralization ability *in vitro* among these three samples and can be regarded as the optimal composition. As mentioned previously, the solidification of the composite bone cement was a result of the Ca^{2+} induced gelation process of sodium alginate. The low chemical durability of the Sol-Gel-derived borosilicate bioactive glasses and resultant rapid Ca^{2+} release, therefore, provided a prerequisite for the gelation. In addition to the glass composition,

their excellent textural properties including high specific surface area and pore volume played an essential role in enhancing the mechanical properties and workability of the bone cements. Also, both factors favored their bioactive response, thus a rapid mineralization rate was observed. These desirable properties indicated that the composite bone cements would be promising candidates for the use in minimally invasive surgery for treatment of bone defects. Furthermore, the exceptional textural properties of the MBGS enable the loading of diverse drugs, thereby achieving a multifunctional task in bone tissue engineering applications. In the future research, improving the compressive strength of mesoporous borosilicate bioactive glass bone cement should be continuously studied to meet the requirement of clinical application.

3 Conclusions

In this study, mesoporous borosilicate bioactive glass spheres with various $\text{B}_2\text{O}_3/\text{SiO}_2$ ratios were prepared by Sol-Gel template method. The resultant glass spheres were then combined with alginate to fabricate injectable composite bone cements. The results indicated that an increase in glass boron content resulted in decreased network connectivity, and thus achieving higher specific surface area and larger pore volume of MBGS, which further accelerated the glass degradation and Ca^{2+} release. It is also confirmed that compared to non-mesoporous bioactive glass used in our previous study, the good textural properties of the mesoporous borosilicate bioactive glass spheres endow the composite bone cements with

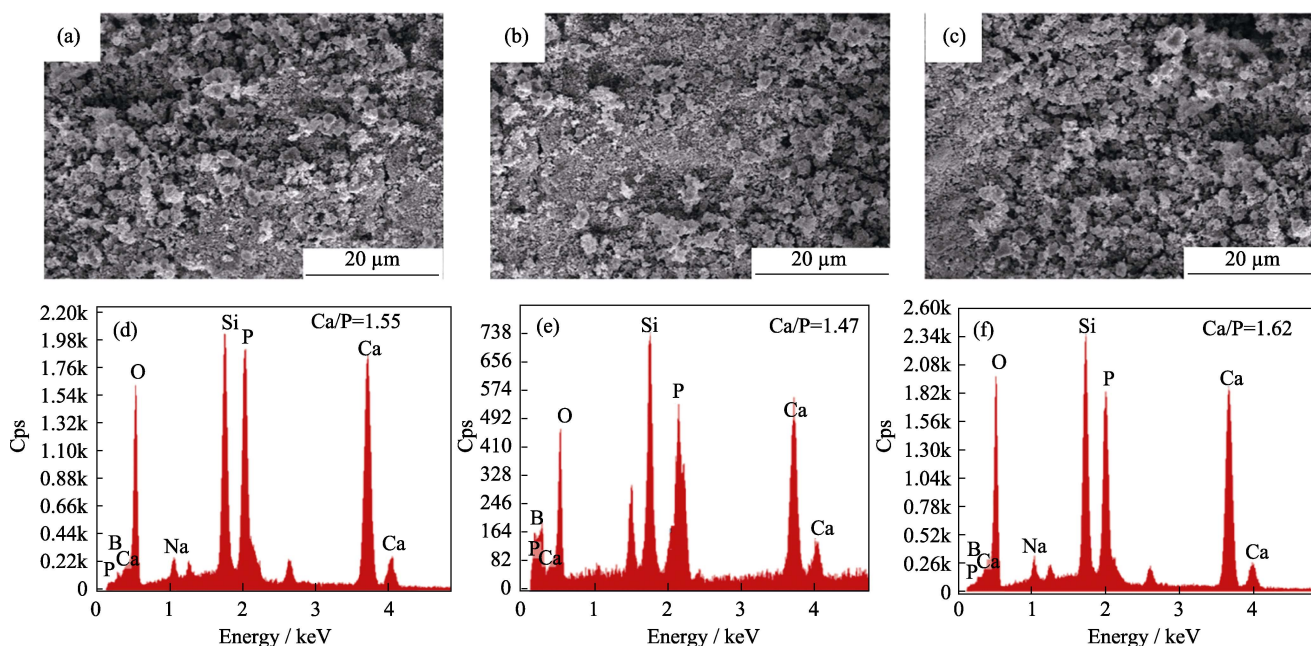


Fig. 12 SEM images and EDS data of (a, d) BC-20, (b, e) BC-30, (c, f) BC-30 after being immersed in SBF for 14 d

improved workability, including clinically appropriate setting time (10–20) min, excellent injectability and anti-washout property, as well as good bioactivity. What's more, BC-30 was the optimal composition for bone cement. Therefore, the present bone cement is a more appropriate option as bone filling and regeneration materials for minimally invasive applications.

References:

- [1] VERRIER S, HUGHES L, ALVES A, *et al.* Evaluation of the *in vitro* cell-material interactions and *in vivo* osteo-integration of a spinal acrylic bone cement. *European Spine Journal*, 2012, **21(6)**: S800–S809.
- [2] KRETLOW J D, KLOUDA L, MIKOS A G. Injectable matrices and scaffolds for drug delivery in tissue engineering. *Adv. Drug Delivery Rev.*, 2007, **59(4/5)**: 263–273.
- [3] LV Y, LI A L, ZHOU F, *et al.* A novel composite PMMA-based bone cement with reduced potential for thermal necrosis. *ACS Appl. Mater. Interfaces*, 2015, **7(21)**: 11280–11285.
- [4] CABANAS M V, RODRIGUEZ-LORENZO L M, VALLET-REGI M. Setting behavior and *in vitro* bioactivity of hydroxyapatite/calcium sulfate cements. *Chem. Mater.*, 2002, **14(8)**: 3550–3555.
- [5] JAMALI A, HILPERT A, DEBES J, *et al.* Hydroxyapatite/calcium carbonate (HA/CC) vs. plaster of Paris: a histomorphometric and radiographic study in a rabbit tibial defect model. *Calcif Tissue Int.*, 2002, **71(2)**: 172–178.
- [6] BOHNER M, BAROUD G. Injectability of calcium phosphate pastes. *Biomaterials*, 2005, **26(13)**: 1553–1563.
- [7] HABIB M, BAROUD G, GITZHOFFER F, *et al.* Mechanisms underlying the limited injectability of hydraulic calcium phosphate paste. *Acta Biomaterialia*, 2008, **4(5)**: 1465–1471.
- [8] HOPPE A, GULDAL N S, BOCCACCINI A R. A review of the biological response to ionic dissolution products from bioactive glasses and glass-ceramics. *Biomaterials*, 2011, **32(11)**: 2757–2774.
- [9] KANG M S, LEE N H, SINGH R K, *et al.* Nanocements produced from mesoporous bioactive glass nanoparticles. *Biomaterials*, 2018, **162**: 183–199.
- [10] CHEN C, LI H, PAN J F, *et al.* Biodegradable composite scaffolds of bioactive glass/chitosan/carboxymethyl cellulose for hemostatic and bone regeneration. *Biotechnol. Lett.*, 2015, **37(2)**: 457–465.
- [11] LI H B, WANG D P, WU Y Y, *et al.* Effect of citric acid concentration on the properties of borate glass bone cement. *Journal of Inorganic Materials*, 2017, **32(8)**: 831–836.
- [12] CUI X, HUANG W H, ZHANG Y D, *et al.* Evaluation of an injectable bioactive borate glass cement to heal bone defects in a rabbit femoral condyle model. *Materials Science & Engineering C-Materials for Biological Applications*, 2017, **73**: 585–595.
- [13] CUI X, ZHANG Y D, WANG H, *et al.* An injectable borate bioactive glass cement for bone repair: preparation, bioactivity and setting mechanism. *Journal of Non-Crystalline Solids*, 2016, **432**: 150–157.
- [14] WU Y Y, YE S, YAO A H, *et al.* Effect of gas-foaming porogen- NaHCO_3 and citric acid on the properties of injectable macroporous borate bioactive glass cement. *Journal of Inorganic Materials*, 2017, **32(7)**: 777–784.
- [15] MOSEMAN R F. Chemical disposition of boron in animals and humans. *Environmental Health Perspectives*, 1994, **102(suppl 7)**: 113–117.
- [16] DELLA PEPA G, BRANDI M L. Microelements for bone boost: the last but not the least. *Clinical Cases in Mineral and Bone Metabolism*, 2016, **13(3)**: 181–185.
- [17] DURAND L A H, GONGORA A, LOPEZ J M P, *et al.* *In vitro* endothelial cell response to ionic dissolution products from boron-doped bioactive glass in the $\text{SiO}_2\text{-CaO-P}_2\text{O}_5\text{-Na}_2\text{O}$ system. *Journal of Materials Chemistry B*, 2014, **2(43)**: 7620–7630.
- [18] YAO A H, WANG D P, HUANG W H, *et al.* *In vitro* bioactive characteristics of borate-based glasses with controllable degradation behavior. *Journal of The American Ceramic Society*, 2007, **90(1)**: 303–306.
- [19] FU Q A, RAHAMAN M N, FU H L, *et al.* Silicate, borosilicate, and borate bioactive glass scaffolds with controllable degradation rate for bone tissue engineering applications. I. Preparation and *in vitro* degradation. *Journal of Biomedical Materials Research Part A*, 2010, **95A(1)**: 164–171.
- [20] FU Q A, RAHAMAN M N, BAL B S, *et al.* Silicate, borosilicate, and borate bioactive glass scaffolds with controllable degradation rate for bone tissue engineering applications. II. *In vitro* and *in vivo* biological evaluation. *Journal of Biomedical Materials Research Part A*, 2010, **95A(1)**: 172–179.
- [21] BROWN R F, RAHAMAN M N, DWILEWICZ A B, *et al.* Effect of borate glass composition on its conversion to hydroxyapatite and on the proliferation of MC3T3-E1 cells. *Journal of Biomedical Materials Research Part A*, 2009, **88(2)**: 392–400.
- [22] TURCO G, MARSICH E, BELLOMO F, *et al.* Alginate/hydroxyapatite biocomposite for bone ingrowth: a trabecular structure with high and isotropic connectivity. *Biomacromolecules*, 2009, **10(6)**: 1575–1583.
- [23] LEE K Y, MOONEY D J. Alginate: properties and biomedical applications. *Progress in Polymer Science*, 2012, **37(1)**: 106–126.
- [24] SCHERDEL C, REICHENAUER G, WIENER M. Relationship between pore volumes and surface areas derived from the evaluation of N_2 -sorption data by DR-, BET- and *t*-plot. *Microporous Mesoporous Mater.*, 2010, **132(3)**: 572–575.
- [25] LANDERS J, GOR G Y, NEIMARK A V. Density functional theory methods for characterization of porous materials. *Colloids and Surfaces a-Physicochemical and Engineering Aspects*, 2013, **437**: 3–32.
- [26] XIE X, PANG L B, YAO A H, *et al.* Nanocement produced from borosilicate bioactive glass nanoparticles composited with alginate. *Australian Journal of Chemistry*, 2019, **72(5)**: 354–361.
- [27] GBURECK U, BARRALET J E, SPATZ K, *et al.* Ionic modification of calcium phosphate cement viscosity. Part I: hypodermic injection and strength improvement of apatite cement. *Biomaterials*, 2004, **25(11)**: 2187–2195.
- [28] CHEN C C, WANG C W, HSUEH N S, *et al.* Improvement of *in vitro* physicochemical properties and osteogenic activity of calcium sulfate cement for bone repair by dicalcium silicate. *Journal of Alloys and Compounds*, 2014, **585**: 25–31.
- [29] O'NEILL R, MCCARTHY H O, MONTUFAR E B, *et al.* Critical review: Injectability of calcium phosphate pastes and cements. *Acta Biomaterialia*, 2017, **50**: 1–19.
- [30] CATAURO M, BOLLINO F, RENELLA R A, *et al.* Sol-Gel synthesis of $\text{SiO}_2\text{-CaO-P}_2\text{O}_5$ glasses: Influence of the heat treatment on their bioactivity and biocompatibility. *Ceramics International*, 2015, **41(10)**: 12578–12588.
- [31] LIU X, RAHAMAN M N, DAY D E. Conversion of melt-derived microfibrillar borate (13-93B3) and silicate (45S5) bioactive glass in a simulated body fluid. *Journal of Materials Science-Materials in Medicine*, 2013, **24(3)**: 583–595.
- [32] CUI J, CAO X, SHI L, *et al.* Influence of the slight adjustment of oxides on the structural and physico-chemical properties of thin film transistor-liquid crystal display substrate glass. *Royal Soc.*

- Open Sci.*, 2020, **7**(1): 191425–1–12.
- [33] ZHANG Y, ZHANG Z F, YAN W, *et al.* Hexagonal mesoporous silica islands to enhance photovoltaic performance of planar junction perovskite solar cells. *Journal of Materials Chemistry A*, 2017, **5**(4): 1415–1420.
- [34] REN X, TUO Q, TIAN K, *et al.* Enhancement of osteogenesis using a novel porous hydroxyapatite scaffold *in vivo* and *in vitro*. *Ceramics International*, 2018, **44**(17): 21656–21665.
- [35] LI S, SONG C, YANG S, *et al.* Supercritical CO₂ foamed composite scaffolds incorporating bioactive lipids promote vascularized bone regeneration via Hif-1 α upregulation and enhanced type H vessel formation. *Acta Biomaterialia*, 2019, **94**: 253–267.
- [36] ZHANG J T, LIU W Z, SCHNITZLER V, *et al.* Calcium phosphate cements for bone substitution: Chemistry, handling and mechanical properties. *Acta Biomaterialia*, 2014, **10**(3): 1035–1049.
- [37] WANG Y, LIAO T, SHI M, *et al.* Facile synthesis and *in vitro* bioactivity of radial mesoporous bioactive glasses. *Materials Letters*, 2017, **206**: 205–209.

基于介孔硼硅酸盐生物活性玻璃微球的可注射复合骨水泥

常宇辰¹, 林子扬¹, 谢 昕¹, 吴章凡¹, 姚爱华¹,
叶 松¹, 林 健¹, 王德平¹, 崔 旭²

(1. 同济大学 材料科学与工程学院, 上海 201804; 2. 中国科学院 深圳先进技术研究院 生物医药与技术研究所 人体组织与器官退化性研究中心, 深圳 518055)

摘 要: 以溶胶-凝胶法制备的介孔硼硅酸盐生物活性玻璃微球(MBGS)作为固相, 海藻酸钠(SA)溶液作为液相, 开发了一种可注射复合骨水泥。对 MBGS 中氧化硼/氧化硅的比例对其质构性能及骨水泥的可操作性、抗压强度和生物活性的影响进行表征。实验结果表明, 随着硼含量的增加, MBGS 的比表面积从 161.71 m²/g 增大至 214.28 m²/g, 平均孔径以及总孔容也随之增长, 加速了玻璃相中钙离子的释放, 使得玻璃与 SA 的快速交联, 改善了骨水泥可操作性能和力学性能, 凝固时间由 21 min 缩短至 9 min, 抗压强度由 3.4 MPa 提升至 4.1 MPa, 体外矿化性能也随之提高。综合各方面性能表现, BC-30 骨水泥兼具良好的可操作性、力学性能和体外矿化能力, 是最合适的骨水泥组分。总之, 提高 MBGS 的质构性能是增强复合骨水泥的可操作性、抗压强度和生物活性的有效方法。

关 键 词: 可注射骨水泥; 介孔硼硅酸盐生物活性玻璃; 生物活性; 可操作性

中图分类号: TQ171 文献标识码: A